Title
A T.E.M. CHARACTERIZATION OF Mo2C PRECIPITATES IN MOLYBDENUM

Author
Lang, J-M.

Publication Date
1982-04-01

LBL-14295

Lawrence Berkeley Laboratory
UNIVERSITY OF CALIFORNIA

Materials & Molecular
Research Division

A T.E.M. CHARACTERIZATION OF Mo_2C PRECIPITATES IN MOLYBDENUM

Jean-Marc Lang
(M.S. thesis)

April 1982

Prepared for the U.S. Department of Energy under Contract DE-AC03-76SF00098

DISCLAIMER

A T. E. M. CHARACTERIZATION OF Mo_2C PRECIPITATES IN MOLYBDENUM

Master of Science Thesis

Materials Science

Jean-Marc Lang

Materials and Molecular Research Division

Lawrence Berkeley Laboratory

and

Department of Materials Science and Mineral Engineering

University of California

Berkeley, California 94720

April 1982

This work was supported for nine months by an I.R.S.I.D. scholarship and subsequently by the Director, Office of Energy Research, Office of Basic Energy Sciences, Materials Science Division of the U. S. Department of Energy under Contract No. DE-AC03-76SF00098.

A TEM Characterization of Mo_2C Precipitates in Molybdenum

Table of Contents

ABSTRACT

Semicoherent platelets of hcp Mo_2C in a bcc Mo matrix were analysed.

The habit plane was found to be the {301} Mo planes; the precipitate broad faces are covered by one set of dislocations lying along $[\bar{1}13]$ Mo direction; this direction is the calculated line which remains invariant in the transformation from the bcc to the hcp lattice.

The Orientation Relationship is close to the Burgers orientation relationship with an additional rotation bringing (101)(Mo) and $(\bar{1}011)Mo_2C$ into coincidence. Due to this rotation two variants are in twin relation and it was found that these two variants grew together.

1. INTRODUCTION

The orientation relationship and relative morphology of two different phases has strong consequences on the microstructure, hence the properties of a material. In solid state transformation, different approaches such as Eshelby's elasticity theory (1), Bollman's O-lattice (2) and martensite theory (3) have been used.

Eshelby's theory minimises the strain associated with a coherent inclusion in the crystal reduced to an elastic continuum to predict a habit plane. On the other hand, Bollman's O-lattice does take into account the crystallographic nature of the problem since it optimises the dislocation content of the interface between two phases. In a similar way, martensite theory calculates a mobile and macroscopically distortion-free habit plane.

Dahmen and Westmacott (4) have shown that when plotted on stereograms, the results of these apparently different theories are strikingly similar and point

to a common factor which was shown to be the existence of a line which remains invariant during the transformation. For example, if the invariant line was a crystallographic direction, the atoms lying on this direction would not move during the general shuffle producing one crystal structure from the other.

If the existence of an invariant line (I.L.) is taken as a first principle in phase transformation, Dahmen (5) has shown that the O.R. of precipitates can be accurately predicted. This theory has been particularly successful in explaining, for example, the different O.R. of Mo_2C in a Mo matrix or in a Fe matrix. In the first case the ratio of the lattice parameters of the hexagonal phase (Mo_2C) to the bcc phase (Mo) is such that an invariant line (I.L.) can be produced by a 5.26° rotation around $[011]_{Mo}$ yielding the Burgers O.R. In the case of an Fe matrix, the lattice parameters are such that an I.L. cannot be produced and the Mo_2C precipitates have an unrotated O.R. with the Fe matrix (Pitsch-Schrader O.R.)(6).

The axis of apparently random bcc Cr needles in a fcc Cu matrix has been rationalized by this theory (4). When the needles are coherent, they orient themselves in order to minimize the strain energy, that is they lie along the possible I.L. As the strain energy is a continuum concept, these possible I.L. build, in fact, a continuous cone. Experimentally, coherent Cr needles were actually found to lie on such a cone. However, an additional requirement is necessary for the loss of coherency; the transformation strain has to be relieved and for that it has to be close to the direction of an available Burgers vector of the Cu matrix; this crystallographic, hence discrete, requirement determines uniquely the possible axes for semi-coherent needles to be the <761> directions. This was experimentally confirmed and the needles were found to cluster around <110> directions which are the Burgers vector directions in a Cu matrix.

The I.L. theory is also helpful in predicting the ideal structure of a semi-coherent interface. O-lattice theory can give an estimate of the interfacial

energy, and it can be shown (7) that the optimum interface has only one set of dislocations which are parallel to the I.L.. This was verified for the bcc to hcp massive transformation in Al-Ag alloys (8).

These examples show that the I.L. hypothesis is quite satisfactory in predicting O.R.'s in the case of bcc to hcp phase transformation in interstitial (Mo-C) and substitutional (Al-Ag) alloys. It is as successful for the study of the bcc/fcc and bcc/hcp interfaces in substitutional alloys (Cu-Cr, Ag-Al alloys).

The purpose of this research was to investigate the precise O.R., and the structure of a bcc/hcp interface for an interstitial alloy and to test the I.L. hypothesis and its consequences in this particular case.

The Mo-C system was chosen since semi-coherent platelets form after a quench-aging heat-treatment (9). This system is also well-documented as will be shown in the brief literature survey.

2. A BRIEF LITERATURE SURVEY of the Mo-C System

Bürck (9) has presented an extensive and precise study of the evolution of the microstructure of rapidly quenched Mo-C alloys with different heat treatments. His samples were quenched from 2600K in a Ga-In liquid bath to prevent heterogeneous nucleation. At temperatures above 900K the supersaturated solid solution decomposes into small platelet precipitates showing a loop-like contrast in TEM; according to Bürck these precipitates have (114) habit planes and are coherent. When annealed at a higher temperature (1100K), the precipitates are semi-coherent platelets associated with matrix dislocations. The interface structure and the habit plane was not specified. These are the precipitates analyzed in the present study.

Precipitation of group IVA carbides and nitrides (TiC, TiN, ZrC, ZnRn HfN, HfC) in molybdenum has been studied by Ryan, Soffa and Crawford (10). These six compounds have the NaCl face centered cubic structure. Zirconium and

hafnium carbides and nitrides lie on {100} planes; however, the titanium carbides and nitrides have a {301} habit plane, a result similar to the one reported in the present study.

The first stages of precipitation of molybdenum carbides in a molybdenum matrix have been studied by means of electrical resistivity and transmission electron microscopy by Bürck (9,11) and Yoshioka and Kimura (12,13). These results, though very interesting in terms of carbon-vacancy co-precipitation will not be detailed here.

Kumar and Eyre (14) were interested in the role of interstitial elements on the deformation and fracture of group VIA metals and more specifically in the role of Mo_2C precipitates heterogeneously nucleated in a Mo matrix. They studied the suppression of intergranular fracture by precipitation of semi-coherent carbides at grain boundaries. In the course of this investigation, they analysed the O.R. between carbides and matrix. They found an approximate Burgers O.R..

3. EXPERIMENTAL PROCEDURES

The materials were prepared from Molybdenum ribbons supplied by Johnson, Matthey and Co.. The main impurities are iron (< 20 at ppm) and chromium (< 10 at ppm). Interstitial impurities are carbon, nitrogen and oxygen which are at a level less than 100 at ppm in the untreated samples. The strips were rolled down to a thickness of 150μm, and homogenized by joule heating in an ultra-high vacuum furnace (10^{-8} torr) at 2600K. The details of the device are described in Ref. (15). During such a heat treatment oxygen, nitrogen and hydrogen outgas to levels below 10 at.ppm (9). At the same time the rolled strip recrystallizes into large grains with a preferred orientation so that the [100] axis is perpendicular to the plane of the foil. The specimens were then heated to 1900K in a known volume of acetylene ($\sim$ 1ℓ) at a given pressure (10^{-4} torr). This

process ensures an estimated carbon concentration of 500 to 5000 at ppm and is sufficient to study structural features of precipitation but totally inadequate for quantitative studies.

To prevent heterogeneous nucleation on grain boundaries, the sample was quenched by switching off the heating current. The cooling rate was measured with a 75µm tungsten-rhenium thermocouple and an oscilloscope. It was found to be $\simeq$ 2500Ks^{-1}. In the same UHV system the specimens were then annealed for 1 hr at 1073K.

Electropolishing

From the carburized and annealed strip 2.3mm discs were punched out and electropolished in a methanol, glycerol, sulfuric acid (80%, 16%, 4%) solution. The temperature was -35°C, the voltage 30V. Adding glycerol resulted in a slower but better polish, and reduced the preferential etching of big Mo_2C precipitates. When using more glycerol, one has to increase the temperature and decrease the voltage.

Electron Microscopy

A Philips 301 was used for conventional microscopy, a JEOL 200CX for high resolution, a Philips 400 for convergent beam experiments, and the new 1.5MeV Kratos HVEM to obtain good penetration in thick foils.

4. EXPERIMENTAL RESULTS

4.1. Orientation Relationship

As small precipitates give very weak diffraction information, it is helpful to use the bcc Mo matrix diffraction spots for tilting experiments on the hcp Mo_2C precipitates, and thus the knowledge of the orientation relationship is essential. The convergent beam technique was used on relatively big precipitates protruding from the edge of the foil. The size (500Å) and the convergence angle

(5.10^{-3}rd) of the electron beam is such that Kikuchi lines are obtained from the precipitate only, which can then be oriented along a low order zone axis with very good precision (Fig. 1). The probe is then set on the nearby matrix without moving the specimen. The relative orientation is then determined with an accuracy of at least 0.5° (16).

In the case of Fig. 1, the use of a short camera length shows very clearly the "distance" between the $[001]_{Mo}$ and $[11\bar{2}0]_{Mo_2C}$ axes. This distance corresponds to a rotation of $5.5 \pm 0.5°$ around the $[110]_{Mo}$ axis. The orientation is the Burgers relationship as was reported by [14]. These authors detected by analysis of moire patterns a misalignment of $[110]_{Mo}$ and $[0001]_{Mo_2C}$. This can be precisely measured and visualized by a high resolution lattice image of a precipitate interface (Fig. 1c) and was found to be 2°. A similar result was reported in the Ta-C system by (5,15). The results are summarized by a double-stereogram in Fig.2 drawn for the relevant $(\frac{c}{a})_{Mo_2C} = 1.57$ ratio. These results were found to be true for smaller platelike precipitates as Fig. 5f obtained by microdiffraction shows.

4.2. Morphology of the semicoherent carbides

Fig. 3a shows the microstructure of hcp Mo_2C platelets in the bcc Mo matrix. Typical dimensions are 0.5µm in diameter and 20nm in thickness. The habit plane was determined by tilting the precipitates edge-on. As the density of platelets is rather low, the improved penetration offered by high voltage microscopy is helpful to select a precipitate suitable for analysis. Moreover, it is easier to decide when a large, rather than thin, section of a precipitate is edge-on. Precision was increased by imaging under weak beam conditions to eliminate the strain contrast surrounding the plates.

In Fig. 3 one can see that one platelet is edge-on for both beam directions $[\bar{1}03]$ and $[\bar{1}13]$; the habit plane is thus uniquely determined to be $(301)_{Mo}$.

The broad faces of the precipitates are covered with an array of remarkably straight lines (Figs. 3, 4). Knowing that they are located in the interface, they were determined to lie along $[\bar{1}13]_{Mo}$ by trace analysis (for example, in B = [013], they are parallel to [200]).

Fig. 4 shows a high magnification picture of one such nearly face-on platelet. The lines are paired corresponding to the top and bottom of the precipitate. One can see an indentation at the edge and a "nose" out of the plane of the precipitate. These last features were quite often observed.

4.3. Analysis of the Interfacial Lines

The strain in the matrix neighboring the platelet can be analysed by classical $\underset{\sim}{g}.\underset{\sim}{b}$ experiment, as is shown in Figs. 5a,b,c. The lines are visible when using the 002 reflection (a) but are out of contrast when using a $03\bar{1}$(b) and an 020 (c) reflection. Thus, the strain in the matrix has a displacement vector with a strong component along [001]. The remainder might be along [100] since it is invisible with beam directions close to [100].

The contrast behavior of the precipitate itself is totally obscured by matrix effects (moire, strain) but valuable information can be gained by microdiffraction.

Fig. 5f is the microdiffraction pattern of Fig. 5e. It can be seen that $[\bar{1}13]_{Mo} = [\bar{1}100]_{Mo_2C}$ = B (beam direction) and that there is a rotation along this axis so that [0001] is not exactly parallel to [110] as has been noted for bigger precipitates. In Fig. 5e the precipitate is seen edge-on along $[\bar{1}13]$ which is the direction of the interfacial lines. The section of the platelet is striated with lines perpendicular to the [0001] direction.

From this $[\bar{1}100]$ zone, the precipitate has been tilted to $[\bar{2}110]$ using the matrix reflections as a navigational aid. The $[\bar{2}110]$ pattern, instead of well-defined spots, consists of streaks perpendicular to the (0001) plane, with no spots

or streaks in the row passing through the forward scattered beam and parallel to these.

This situation can be analysed in the way proposed by (17). Instead of describing separately matrix and precipitate spots, these can be described as product and parent lattices related by a shear; in the reciprocal lattice the invariant plane has a normal $\vec{s}$, and a shear direction $\vec{n}$ which corresponds in the direct lattice to a shear of direction $\vec{s}$ leaving a plane of normal $\vec{n}$ invariant.

Fig. 5d can be interpreted in real space as a shear along $[\bar{1}100]$ in the plane [0001]. Streaks instead of spots are observed because the shear $\vec{s}$ is not of well-defined magnitude.

This whole tilting and diffraction experiment is summarised in the stereogram of Fig. 6.

4.4 Twin Relation of Double Precipitates.

Many precipitates are paired as is shown, for example, in Fig. 8; that is, two variants grow together. The habit plane and the line direction for these precipitates were determined by stereo and trace analysis; they were found to be respectively $(03\bar{1})$, $[\bar{1}13]$ and (130), $[3\bar{1}\bar{1}]$. Given the dislocation line direction of a plate, the corresponding variant can be uniquely determined since any given <113> direction is contained in only one {110} which is nearly parallel to the unique (0001) basal plane of the precipitate.

The results of Fig. 8 are plotted on a composite stereogram in Fig. 9. One can see that the two variants are related by twinning on the $(\bar{1}101) = K_1$ plane which is exactly parallel to $(101)_{Mo}$.

4.5. Dislocations in the matrix associated with the precipitate.

Many of the precipitates are hidden in a tangle of dislocations which makes a detailed analysis difficult. However, two types of commonly observed dislocations have been distinguished.

The first type consists of dislocation loops lying in planes (probably 110) near the habit plane {301} of the precipitate. These dislocations were always found to have a $\frac{a}{2}$<111> type Burgers vector, and they are pinned at the edges of the platelet. Figs. 10a,b,c show examples of these dislocations; the arrows show small loops being punched out from the edges. Fig. 10c shows how the dislocations are in planes near the habit plane which is edge-on here.

The second type is less often observed probably due to the fact these dislocations are not pinned by the precipitate and can easily glide out. These dislocations are nearly perpendicular to the platelets. Their Burgers vectors were found to be either $\frac{a}{2}$<111> or $\frac{a}{2}$<100>. Figs. 10d,e,f show such an example.

5. DISCUSSION

5.1. Invariant Line

As this research follows logically the work by Dahmen (5,7), and Dahmen and Westmacott (4), the relevant results of the Invariant Line Theory will first be summarized.

It is well known that the Bain strain transforms an fcc into a bcc unit cell by a contraction along the $[001]_{fcc}$ axis and a uniform expansion of the $(001)_{fcc}$ plane (18). The other fcc/bcc O.R.s can be derived from the basic O.R. by rotation around the proper axis (5).

Similarly, as shown in Fig. 7, an hcp cell can be produced out of a non-primitive bcc cell (9). In this case, the equivalent of the Nishiyama-Wasserman O.R. is the Pitsch-Schrader O.R. This transformation is detailed here for the $Mo\text{-}Mo_2C$ ($a_{bcc} = 3.147\mathring{A}$, $a_{hcp} = 3.002\ \mathring{A}$, $c_{hcp} = 4.720\mathring{A}$, $\frac{c}{a} = 1.57$) case. The transformation matrix A refers to the axes

$$(x, y, z) = ([00\bar{1}]_{bcc}, [\bar{1}10]_{bcc}, [110]_{bcc})$$

$$= ([2\bar{1}\bar{1}0]_{hcp}, [01\bar{1}0]_{hcp}, [0001]_{hcp}) .$$

$$A = \begin{pmatrix} \frac{\ell[2\bar{1}\bar{1}0]}{I[00\bar{1}]} & 0 & 0 \\ 0 & \frac{\ell[01\bar{1}0]}{I[\bar{1}10]} & 0 \\ 0 & 0 & \frac{\ell[0001]}{\ell[110]} \end{pmatrix}$$

where $[hk.\ell]$ is the distance between nearest neighbors in the $[hk.\ell]$ direction. In our case.

$$A = \begin{pmatrix} 0.95 & 0 & 0 \\ 0 & 1.17 & 0 \\ 0 & 0 & 1.11 \end{pmatrix} = \begin{pmatrix} a & 0 & 0 \\ 0 & b & 0 \\ 0 & 0 & c \end{pmatrix}$$

a, b, c being constants defined by this relation.

An invariant line can be obtained by a rotation of angle θ, to be determined, around the z = [110] bcc axis. This can be expressed by

$$A' = \begin{pmatrix} \cos\theta & \sin\theta & 0 \\ -\sin\theta & \cos\theta & 0 \\ 0 & 0 & 1 \end{pmatrix} \cdot \begin{pmatrix} a & 0 & 0 \\ 0 & b & 0 \\ 0 & 0 & c \end{pmatrix} = \begin{pmatrix} a\cos\theta & b\sin\theta & 0 \\ -a\sin\theta & b\cos\theta & 0 \\ 0 & 0 & c \end{pmatrix}$$

and $A'\underset{\sim}{u} = \underset{\sim}{u}$, that is det $|A' - I| = 0$ for a nontrivial solution (5). When solved, this equation gives $\cos\theta = \frac{1 + ab}{a+b} = 9.963 \times 10^{-1}$, $\theta = 4.9°$

$$A' = \begin{vmatrix} 0.950 & -0.098 & 0 \\ 0.081 & 1.164 & 0 \\ 0 & 0 & 1.11 \end{vmatrix}$$

The solution of the equation $A'\underset{\sim}{u} = \underset{\sim}{u}$ is the vector

$$\begin{vmatrix} -0.90 \\ 0.43 \\ 0 \end{vmatrix}$$

in the (x, y, z) axis or $[\bar{1}13]_{Mo}$ in the crystallographic axis,

$$\frac{[\bar{1}13][00\bar{1}]}{\sqrt{1+1+9}\sqrt{1}} = -0.90,$$

$$\frac{[\bar{1}13][110]}{\sqrt{1+1+9}\sqrt{1+1}} = +0.43\ ;$$

$$\frac{[\bar{1}13][110]}{\sqrt{1+1+9}\sqrt{1+1}} = 0\ .$$

An invariant line is thus produced by rotation around $[110]_{Mo}$ of 4.9° instead of 5.26° corresponding to the Burgers O.R. Such a difference is just at the limits of experimental precision. It has also been proved that the Invariant Line is the $[\bar{1}13]$ direction, which is the direction of the straight lines observed in the interface of Mo_2C platelets.

At this point it is necessary to discuss the structure of an ideal semi-coherent interface, that is of lowest energy. O-lattice theory permits the

calculation of the structure of a given interface between two phases in a given O.R. A general interface contains two sets of dislocations of Burgers vector and spacing $(\underset{\sim}{b}_1, d_1)$, $(\underset{\sim}{b}_2, d_2)$.

An "energy parameter" $P = (b_1/d_1)^2 + (b_2/d_2)^2$ can be attributed to the interface. Dahmen (7) has shown that this energy can be minimized by letting one spacing go to infinity, that is minimizing the O-lattice unit cell. $\underset{\sim}{b}_i / d_i$ is a measure of the transformation strain in the direction of $\underset{\sim}{b}_i$; for example, a large strain along $\underset{\sim}{b}_i$ would require many dislocations to be accommodated, hence a small spacing and a large value of $\underset{\sim}{b}_i / d_i$. P is minimized by altering the O.R. so that the strain $\underset{\sim}{b}_i / d_i$ goes to zero, which is equivalent to having perfect atomic fit in the direction of $\underset{\sim}{b}_i$. This is the requirement for an Invariant Line and it is demonstrated that the optimum boundary contains a single set of dislocations parallel to the Invariant Line.

The problem can also be tackled in a different way. In the O-lattice treatment no question is asked about the origin of the dislocations; they are just used in the best way to minimize an interface energy. Dahmen and Westmacott (4) have shown that in the case of Cr(bcc) needles in a Cu(fcc) matrix, only those precipitates which have their transformation strain in the direction of an available matrix Burgers vector will grow. The transformation matrix A can be decomposed in a pure deformation matrix P and a shear matrix S. If this shear $\vec{s}$ is in the direction of a parent lattice translation, it can be relieved by the introduction of a set of screw dislocations which constitutes the loss of coherency. As shown by (4) the strain to be accommodated elastically is reduced to $A.S^{-1} = P.S.S^{-1} = P$.

With this theoretical background, the present results can be interpreted in the following way: the straight paired lines are dislocation loops parallel to the Invariant Line; their shear component is along $[1\bar{1}00]_{Mo_2C}$ which is parallel to

$[\bar{1}13]_{Mo}$ as can be seen from the diffraction pattern (Fig. 5d), the bright field images (Fig. 5e) and the indentation (Fig. 4). The loss of coherency is obtained by glide of matrix dislocations, such as the one analysed in Fig. 9d,e,f into the interface, on the nearly parallel $(110)_{Mo}$ and $(0001)_{Mo_2C}$ glide planes.

Since there is a volume change, equal to the determinant of A (23%), the pure deformation P is not the identity, and one expects an elastic strain field in the matrix perpendicular to the I.L. This explains why the strain field in the matrix near the precipitate has a displacement vector along $[100]_{Mo}$ (Figs. 5a,b,c); that is, it has a component perpendicular to $[1\bar{1}00]_{Mo_2C}$ = I.L. (Fig. 6). This strain can occasionally be relieved by glide in the $(110) \simeq (0001)_{Mo_2C}$ plane leading to the formation of "noses" (Fig. 4).

5.2. Twin Relation of Double Precipitates

The two twin-related variants are derived from each other by a mirror operation on $K_1 = (\bar{1}011)_{Mo_2C}$. By definition two variants are related by a symmetry operation of the matrix. Hence K_1 has to be parallel to a mirror plane of the matrix. In a Burgers O.R., this is not the case, but $(101)_{Mo}$ planes are close to $(\bar{1}011)$ planes. However, a rotation of 1° around $[\bar{1}13] = [\bar{1}100]$ will bring the two poles into coincidence (Figs. 2-8); by the same operation (110) and (0001) are no longer parallel which is experimentally observed.

This $K_1 = (1\bar{1}01)$ and $\eta_1 = (1\bar{1}02)$ is not very common in hcp materials but has already been observed in big precipitates of Ta_2C in a matrix of Ta (15).

5.3. Future Experiments

Dahmen (5) has shown that the Invariant Line can be a non-rational direction. It would be interesting to verify if this is experimentally true by very careful and precise line direction measurements. In the case of the Ta-C system, the lattice-parameter ratio is such that the I.L. is close to <112> directions. An analysis of semicoherent Ta_2C precipitates would be a very interesting comparative study.

For further study of the loss of coherency, high resolution imaging of the platelets in the same condition as the one presented in Fig. 5e would be very valuable, but difficult from a pure experimental point of view.

Fig. 11 shows the microstructure obtained after a poorly characterized heat treatment. However, it is interesting in two aspects independent of the thermal history. First the picture shows that some precipitates can lose coherency by punching out prismatic loops. This situation could be compared to the case of Cr (bcc) needles in the Cu (fcc) matrix (4); the precipitates would be the equivalent to those Cr needles lying continuously on the cone of unextended lines after an annealing treatment of 2h at 700°C. That is, they only satisfy the requirement for an invariant line but the shear component of the transformation strain is not close to an available Burgers vector. To prove this point, microdiffraction on these precipitates will be necessary. They then lose coherency by punching out edge loops. Edge loops can only be created in pairs of opposite sign whereas shear loops require no counterpart, and hence it is more favorable to nucleate a shear loop rather than a pair of prismatic loops. One can expect these precipitates to disappear for longer ageing heat treatments in the same way as Cr needles cluster around <110> Cu direction; the only precipitates left should be the ones which lose coherency by shear loop, and are presented earlier in this study.

Another interesting aspect of this micrograph is the heterogeneous nucleation of secondary precipitates on the loops (arrows). The same variant of the precipitates nucleate on the exact spot of the loops. If the loops are of pure edge character, the fact that the same position is chosen by the precipitate nucleus on every loop points to a crystallographic influence. This might be related to the splitting of the dislocation into partials at the spot where the dislocation line is in a favorable crystallographic direction. The particles could

then help the transformation from Mo bcc to Mo_2C (h.c.p.) in the same way as a Shockley partial $\frac{1}{6}$<112> transforms fcc into h.c.p. crystals.

The precipitates in Fig. 11b are edge-on and lie on the (310) plane. These planes are expected to be the habit plane of coherent precipitates as has been reported in the Ta-C system (15). This is in contradiction to the results of Bürck who reports that the habit plane is {114}.

ACKNOWLEDGEMENTS

I appreciate the environment provided in Berkeley by Professor G. Thomas and his group. I am particularly grateful to Dr. K. H. Westmacott for suggesting and supervising this research with his motivating enthusiasm. This work would not have been done without Dr. Dahmen who provided the necessary theoretical background during countless, informal, patient and invaluable discussions. Thanks to Dr. A. R. Pelton whose infectious enthusiasm grew exponentially with the proximity of an electron microscope and to D. Ackland for his help in the HVEM. Thanks to Madeline Moore for putting up with another of those Frenchmen and typing this manuscript most efficiently.

It is an impossible task to express my gratitude to Penelope and Ulrich who took care of me when times were hard and both spirit and limbs in casts.

This work was supported for nine months by an I.R.S.I.D. scholarship and subsequently by the Director, Office of Energy Research, Office of Basic Energy Sciences, Materials Science Division of the U. S. Department of Energy under Contract No. DE-AC03-76SF00098.

REFERENCES

(1) J. W. Eshelby, Proc. Roy. Soc. (A) 341, 376 (1957).

(2) W. Bollmann, Crystal Defects and Crystalline Interfaces, Springer, N. Y. (1970).

(3) C. M. Wayman, Introduction to the Crystallography of Martensitic Transformations, McMillan, N. Y. (1964).

(4) K. H. Westmacott and U. Dahmen, Proceedings of the Conf. on Solid-Solid Phase Transf., Pittsburgh, 1982.

(5) U. Dahmen, Acta Metall. 30, 63 (1982).

(6) D. J. Dyson, S. R. Keown, D. Raynor, and J. A. Whiteman, Acta Metall. 14, 867 (1966).

(7) U. Dahmen, Scripta Metall. 15, 77 (1981).

(8) M. R. Plichta and H. I. Aaronson, Acta Met. 28, 1041 (1980).

(9) P. Bürck, D. Ing. Thesis, Dresden, 1978.

(10) N. E. Ryan, W. A. Soffa, and R. C. Crawford, Metallography 1, 195 (1968).

(11) X. Küthe and P. Bürck, Defects in Refractory Metals, S.C.K./C.E.N. Mol. 117 (1972).

(12) K. Yoshioka and H. Kimura, Scripta Metall. 9, 361 (1975).

(13) K. Yoshioka and H. Kimura, Acta Metall. 23, 1009 (1975).

(14) A. Kumar and B. L. Eyre, Acta Metall. 26, 569 (1978).

(15) U. Dahmen, Ph.D. Thesis, Berkeley, 1979, LBL8661.

(16) G. Thomas and M. Goringe, Transmission Electron Microscopy of Materials, p. 124, John Wiley and Sons, Inc., N. Y., 1979.

(17) K. H. Westmacott and U. Dahmen, Proceedings of 10th Int. Congress on Electron Microscopy, Hamburg, 1982.

(18) A. Kelly and G. W. Groves, Crystallography and Crystal Defects, p. 329, Addison-Wesley, Reading, Massachusetts 1970.

(19) Idem. p. 319.

Figure Captions

Fig. 1. Determination by convergent beam and lattice fringe imaging of the precise orientation relationship of an h.c.p. Mo_2C precipitate in a bcc Mo matrix.

Fig. 2. Composite stereogram showing the O.R. between Mo_2C (h.c.p.) ($\frac{c}{a}$ = 1.57) and Mo (b.c.c.).

Fig. 3. Tilting experiment determining the habit plane and the direction of interfacial lines of Mo_2C platelets. (700kV)

Fig. 4. High magnification image of a typical Mo_2C platelet. Arrows show respectively an indentation and a "nose" in the precipitate.

Fig. 5. a), b), c): Analysis of the strain field in the matrix surrounding a platelet. This strain field has a strong component along [100]. d) Microdiffraction along $[\bar{2}110]_{Mo_2C}$ showing evidence of shear in the (0001) plane along the $[\bar{1}100]_{Mo_2C}$ direction. e) Bright field image showing that the shear plane is $(0001)_{Mo_2C}$. f) Microdiffraction of e); the precipitate spots are underlined. The arrow points to the rotation of $(0001)_{Mo_2C}$ away from $(110)_{Mo}$.

Fig. 6. Stereogram summarizing the preceding results. The habit plane of the precipitate is (301), the Invariant Line (arrow) is $[\bar{1}13]_{Mo} = [\bar{1}100]_{Mo_2C}$. This stereogram presents the phases in the Burgers O.R. and doesn't show the misorientation of $(110)_{Mo}$ and $(0001)_{Mo_2C}$ for clarity purposes.

Fig. 7. a) unit cell of the b.c.c. lattice; b) distorted h.c.p. cell picked out of the b.c.c. lattice as in a c) stereogram of the Pitsch-Schrader O.R. (after 18).

Fig. 8. Two precipitates in Twin Relation. The respective I.L. direction are along $[\bar{1}13]$ and $[3\bar{1}\bar{1}]$.

Fig. 9. Stereogram corresponding to Fig. 7; the habit planes [(130) and $(03\bar{1})$], the I.L. directions ($[\bar{1}13]$, $[3\bar{1}\bar{1}]$) are indicated. By mirror operation on $K_1 = (\bar{1}011)$, exactly parallel to $(101)_{Mo}$, $(0001)_{Mo_2C}$ is transformed into $(0001)_T$ near $(01\bar{1})_{Mo}$, and $[\bar{1}13] = [\bar{1}100]$ is exactly transformed into $[3\bar{1}\bar{1}]_{Mo} = [\bar{1}100]_T$.

Fig. 10. a), b) examples of dislocation loops pinned at the precipitate edges. (700kV). c) same type of dislocations, but seen around an edge-on precipitate. d),e),f) analysis of an $\frac{a}{2}[100]$ dislocation which can slip on the nearly parallel (110) and (0001) Mo_2C planes.

Fig. 11. Secondary precipitation on punched out loops (HVEM, 1MeV); in b) one of the rows of loops is out of contrast. Precipitates on the (310) plane are visible. The dotted background is due to radiation damage.

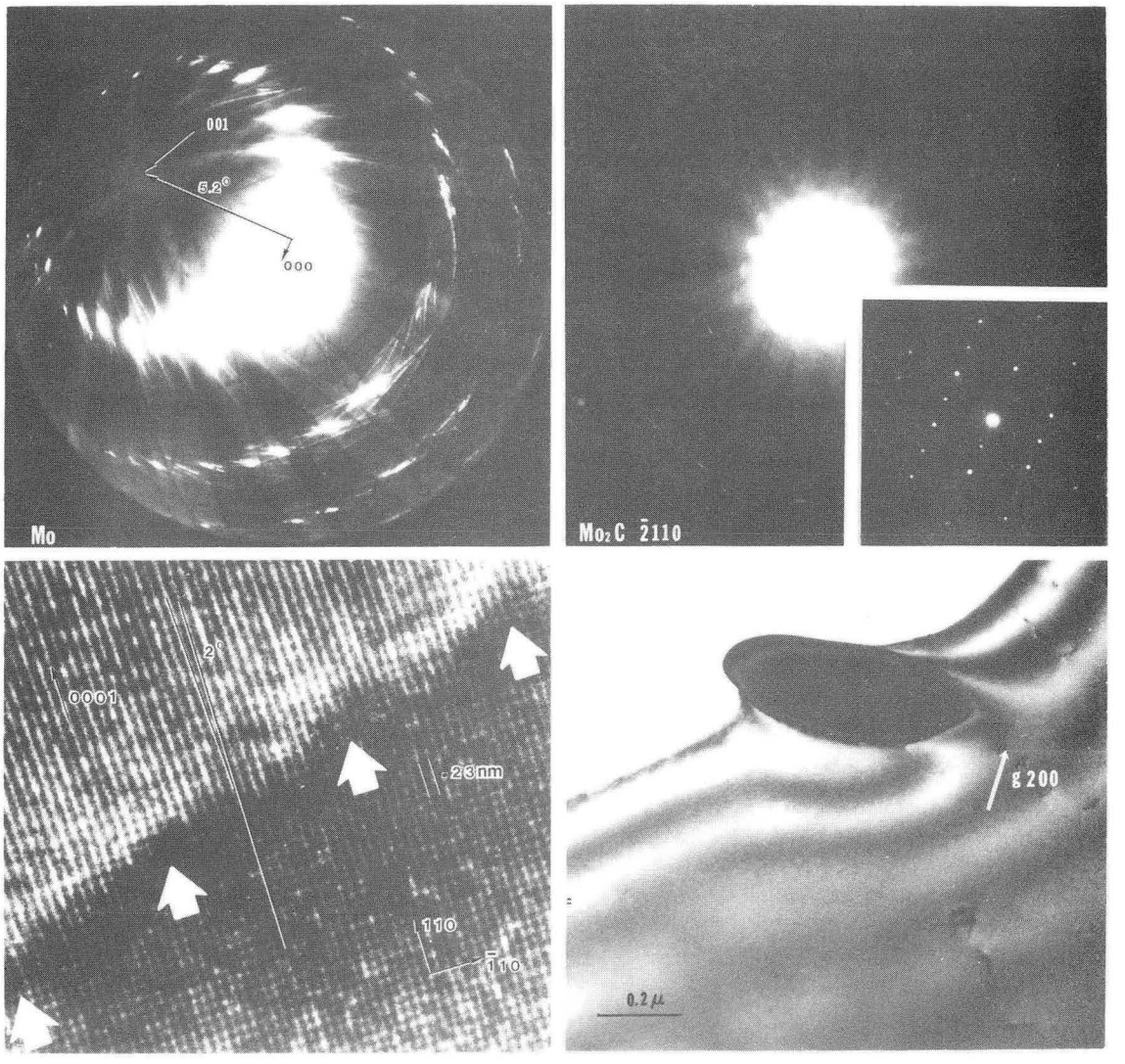

XBB823-2113

Fig. 1

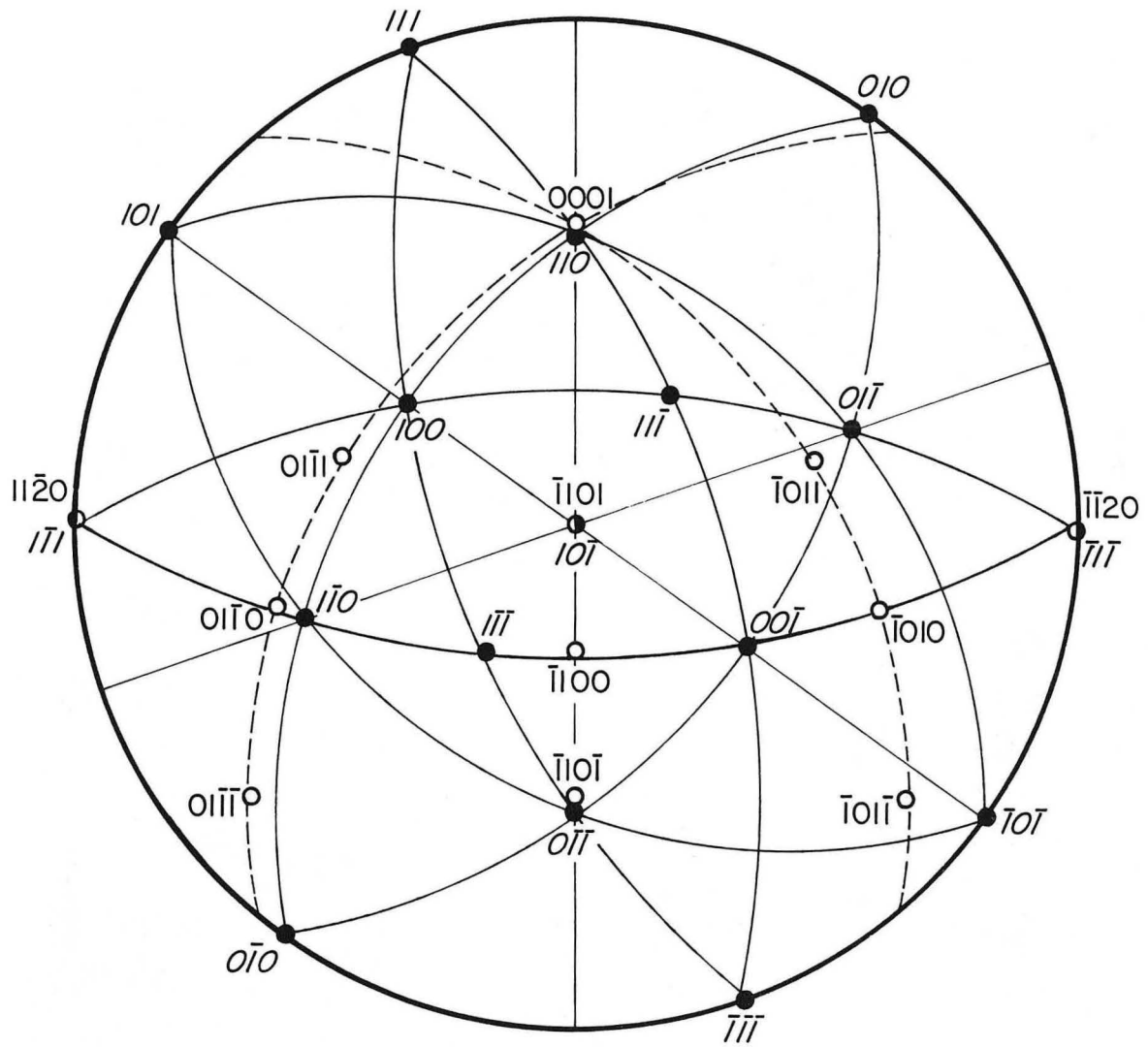

XBL 7811-6083

Fig. 2

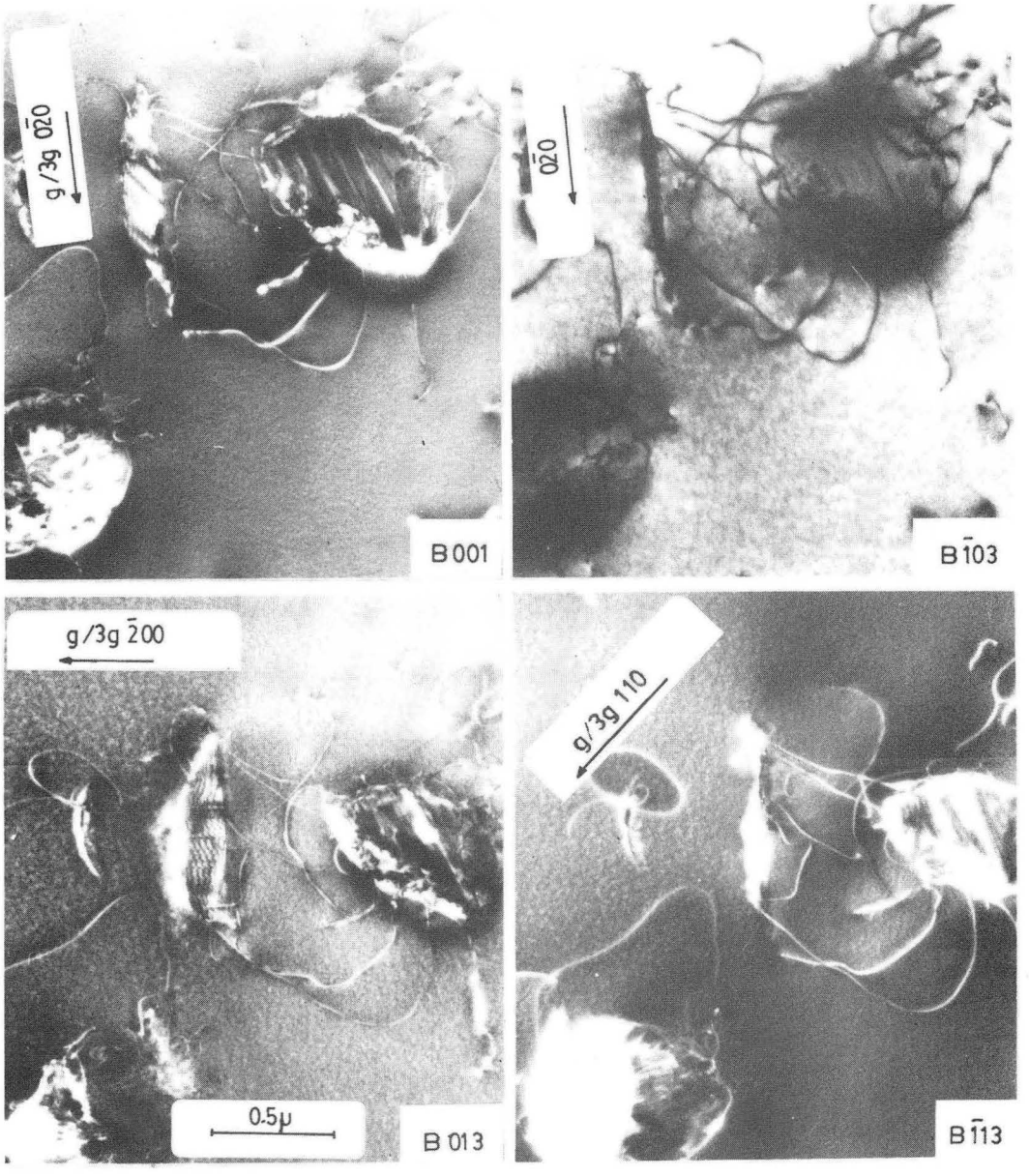

Fig. 3

XBB 823-2111

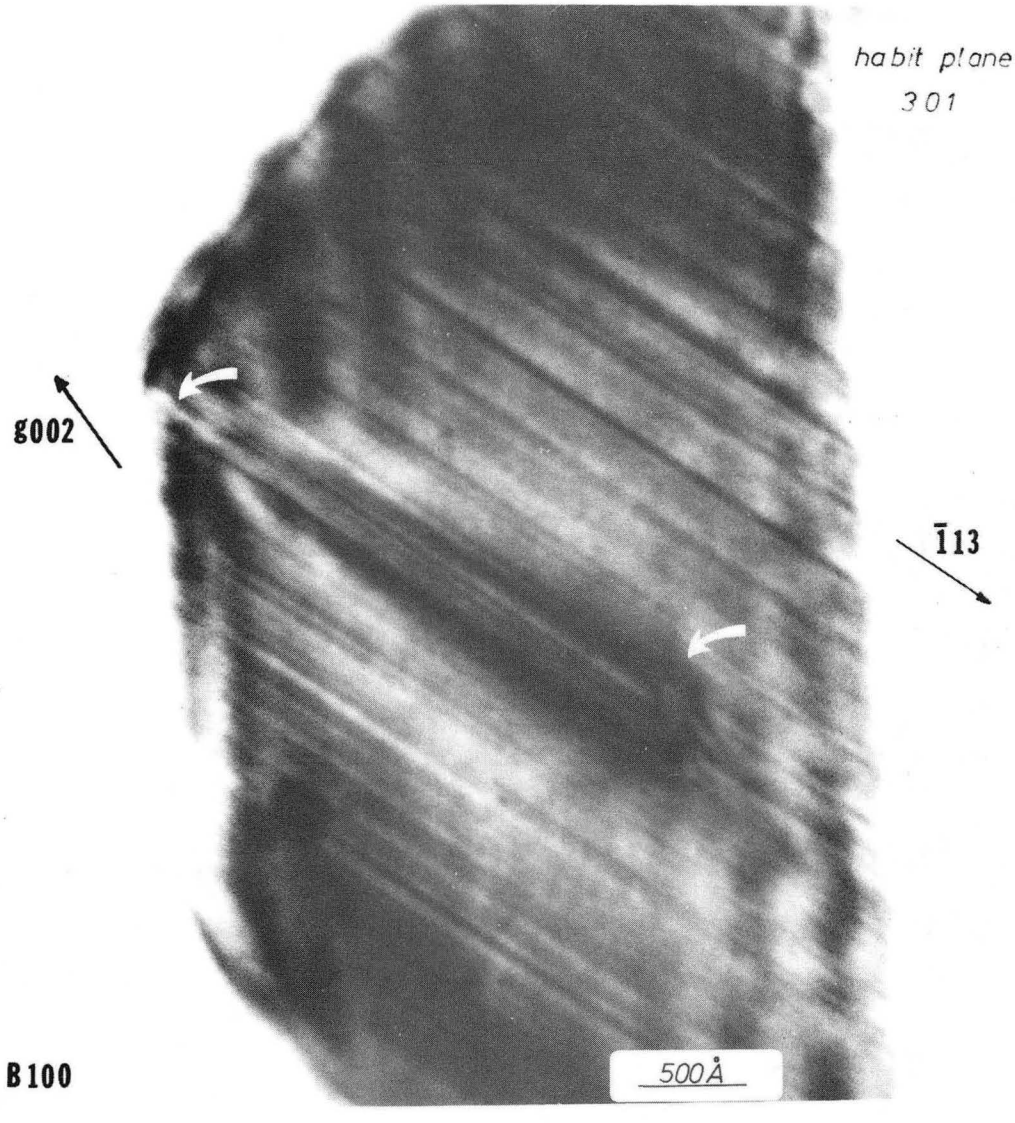

Fig. 4

XBB 823-2109

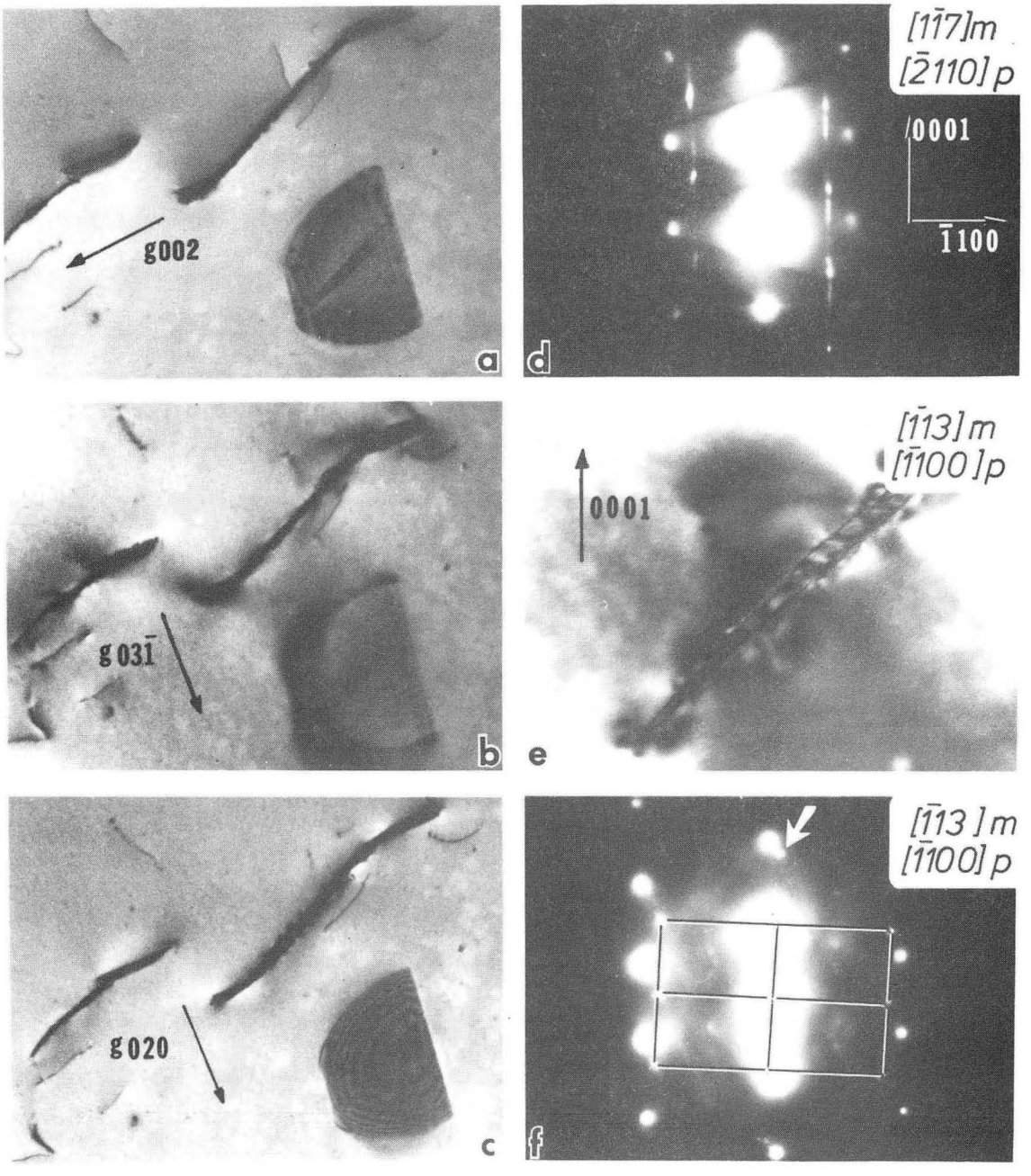

XBB 823-2110A

Fig. 5

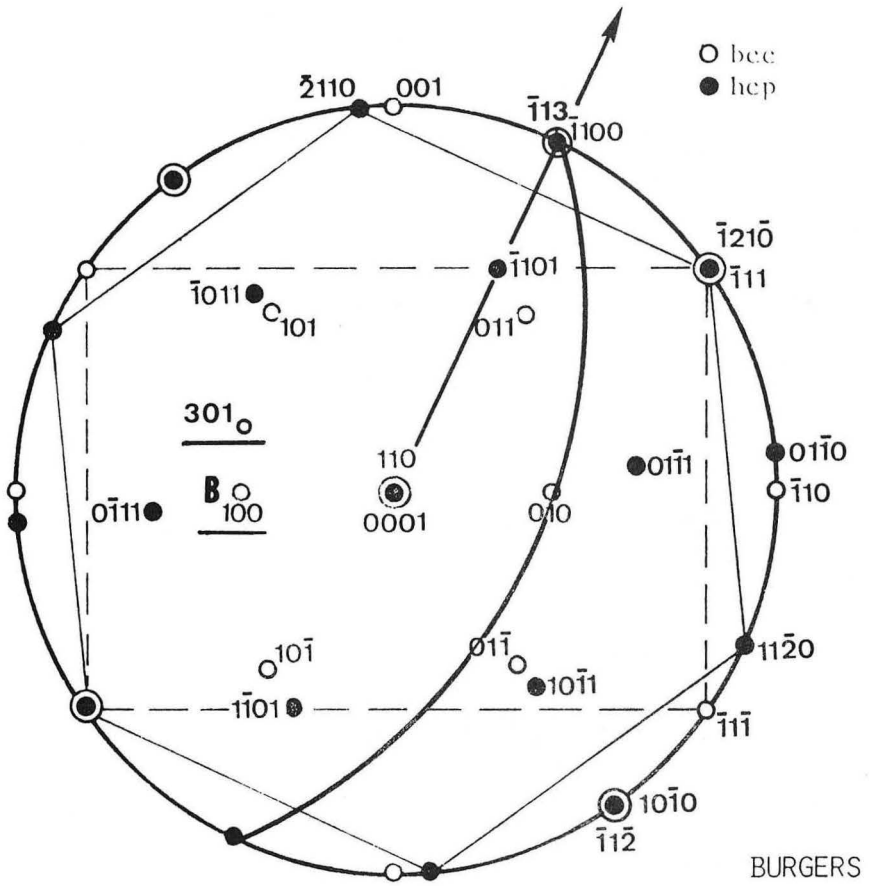

XBL 823-8497

Fig. 6

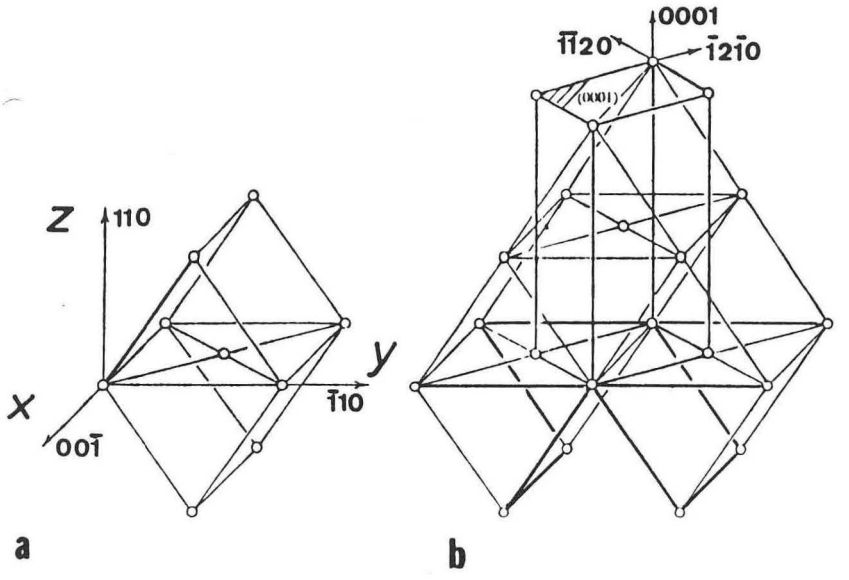

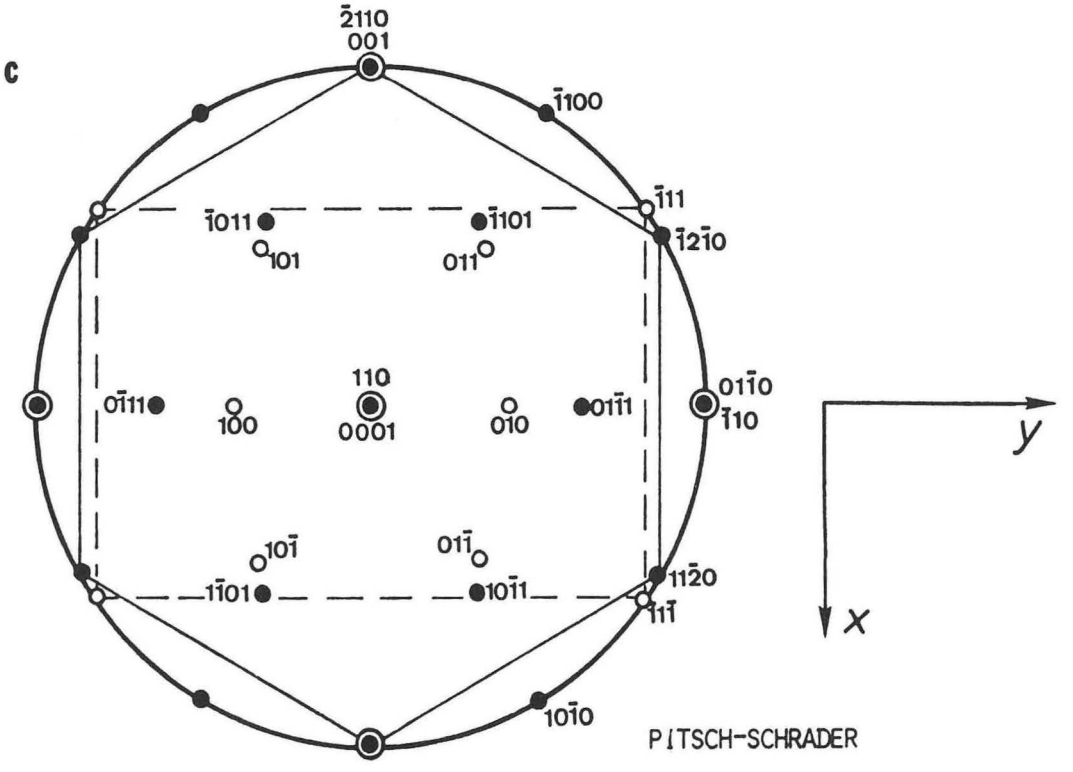

XBL 823-8766

Fig. 7

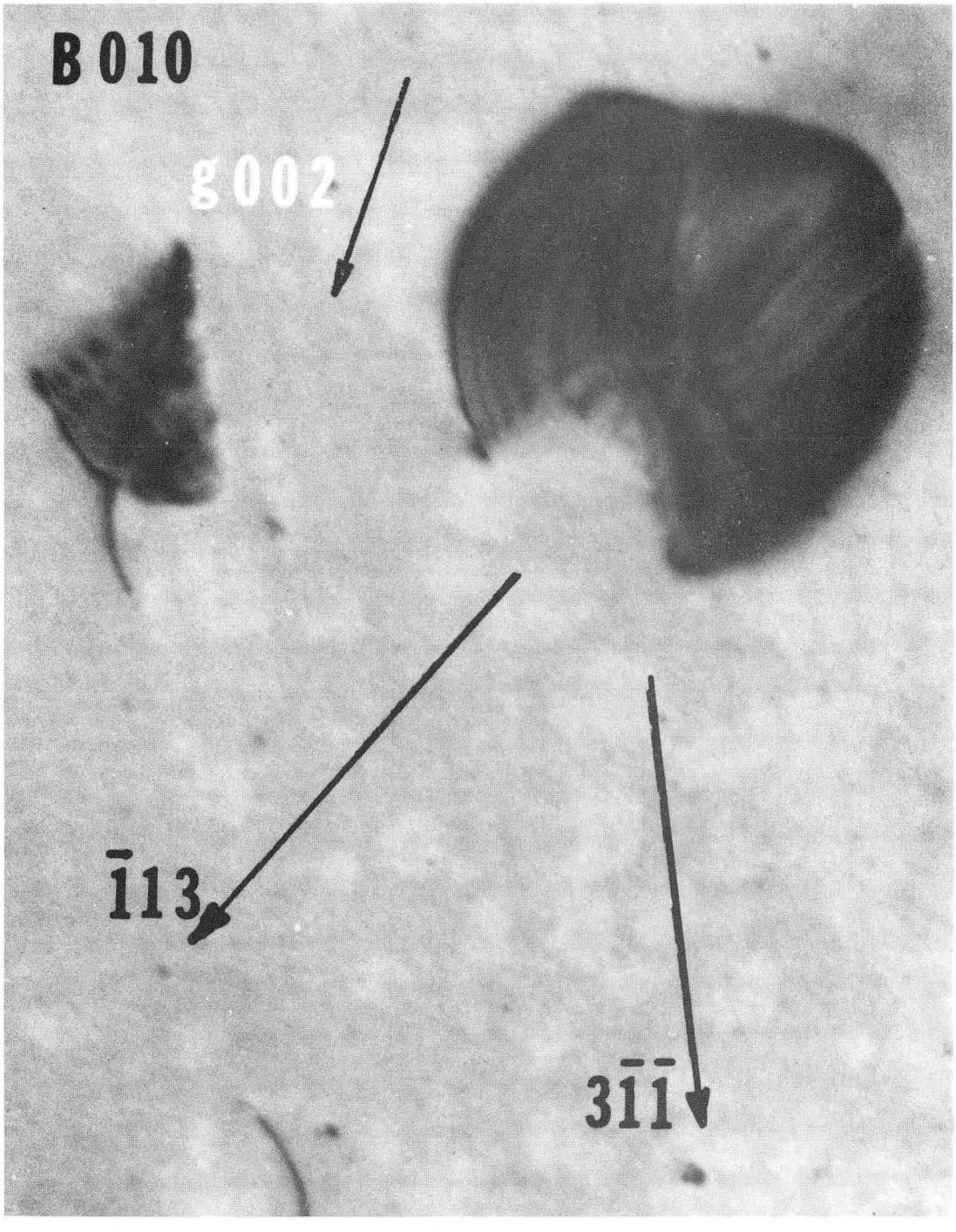

Fig. 8

XBB 823-2108

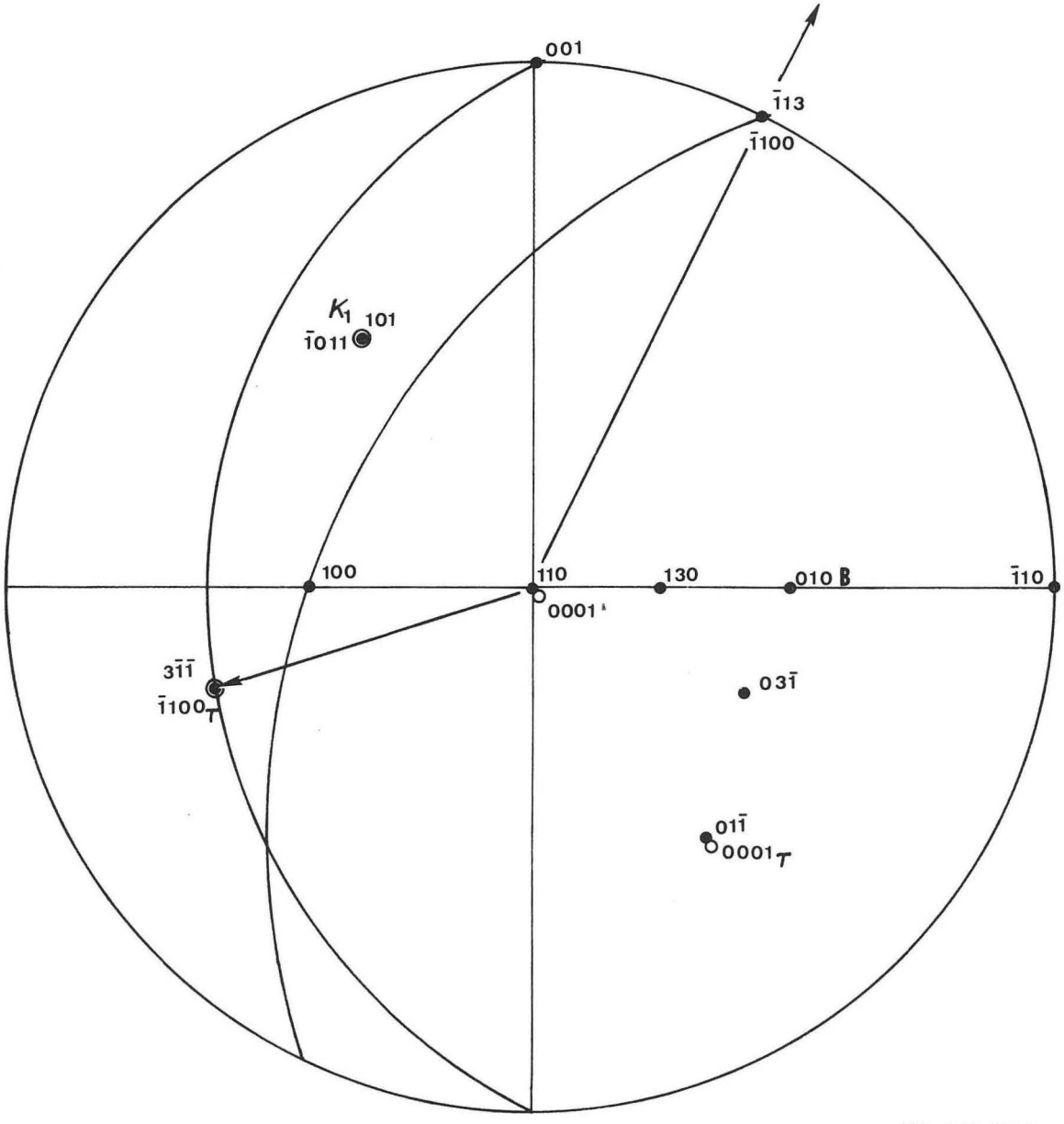
001
$\bar{1}13$
$\bar{1}100$
K_1 101
$\bar{1}011$
100
110
130
010 B
$\bar{1}10$
0001
$3\bar{1}\bar{1}$
$\bar{1}100_T$
$03\bar{1}$
$01\bar{1}$
0001_T
XBL 823-8498

Fig. 9

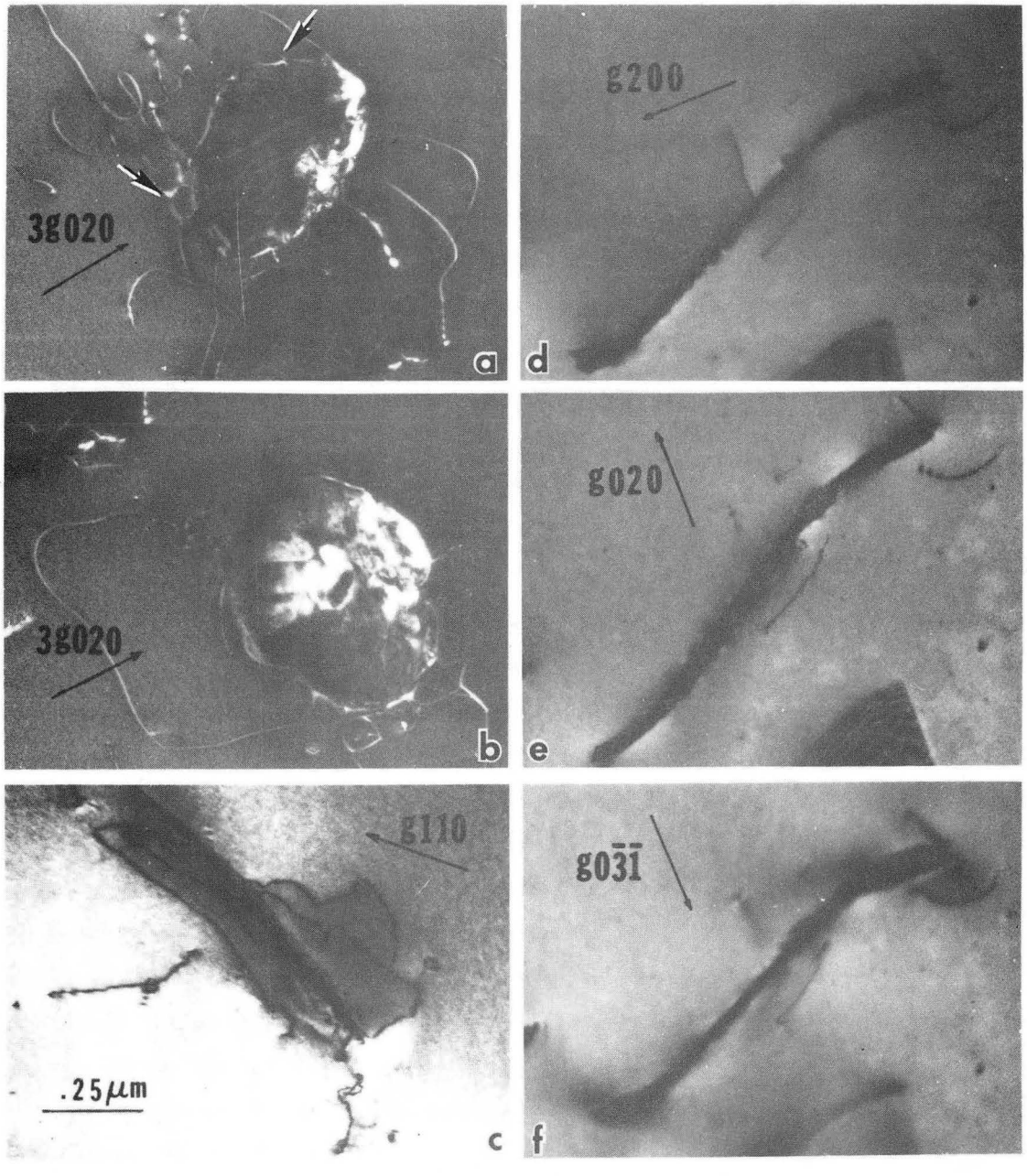

Fig. 10

XBB 823-2112

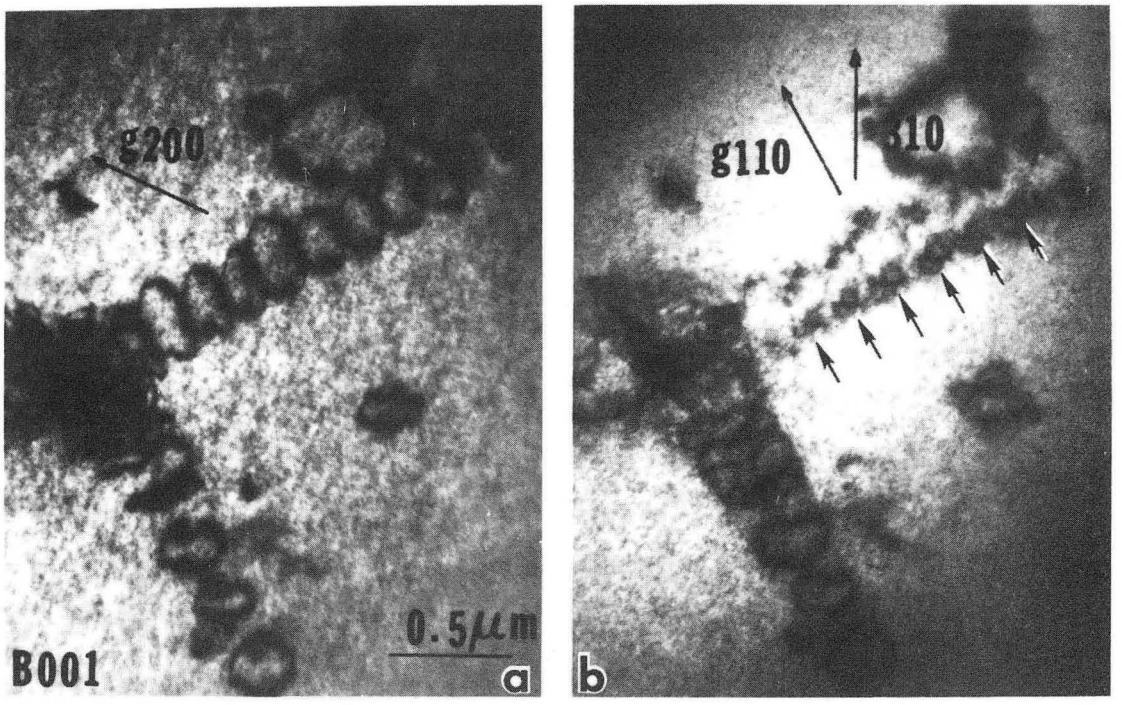

SECONDARY PRECIPITATION ON PUNCHED OUT LOOPS IN Mo-C SYSTEM. HVEM - 1MeV.

Fig. 11

XBB 823-2748

TECHNICAL INFORMATION DEPARTMENT
LAWRENCE BERKELEY LABORATORY
UNIVERSITY OF CALIFORNIA
BERKELEY, CALIFORNIA 94720